1-1-2018

Realization of flat band with possible nontrivial topology in electronic Kagome lattice

Zhi Li
University of Wollongong, zhili@uow.edu.au

Jincheng Zhuang
University of Wollongong, jincheng@uow.edu.au

Li Wang
University of Wollongong, lw037@uowmail.edu.au

Haifeng Feng
University of Wollongong, hf533@uowmail.edu.au

Qian Gao
Nankai University

See next page for additional authors

Realization of flat band with possible nontrivial topology in electronic Kagome lattice

Abstract

The energy dispersion of fermions or bosons vanishes in momentum space if destructive quantum interference occurs in a frustrated Kagome lattice with only nearest-neighbor hopping. A discrete flat band (FB) without any dispersion is consequently formed, promising the emergence of fractional quantum Hall states at high temperatures. Here, we report the experimental realization of an FB with possible nontrivial topology in an electronic Kagome lattice on twisted multilayer silicene. Because of the unique low-buckled two-dimensional structure of silicene, a robust electronic Kagome lattice has been successfully induced by moiré patterns after twisting the silicene multilayers. The electrons are localized in the Kagome lattice because of quantum destructive interference, and thus, their kinetic energy is quenched, which gives rise to an FB peak in the density of states. A robust and pronounced one-dimensional edge state has been revealed at the Kagome edge, which resides at higher energy than the FB. Our observations of the FB and the exotic edge state in electronic Kagome lattice open up the possibility that fractional Chern insulators could be realized in two-dimensional materials.

Disciplines

Engineering | Physical Sciences and Mathematics

Publication Details

Li, Z., Zhuang, J., Wang, L., Feng, H., Gao, Q., Xu, X., Hao, W., Wang, X., Zhang, C., Wu, K., Dou, S. Xue., Chen, L., Hu, Z. & Du, Y. (2018). Realization of flat band with possible nontrivial topology in electronic Kagome lattice. Science Advances, 4 (11), eaau4511-1-eaau4511-7.

Authors

Zhi Li, Jincheng Zhuang, Li Wang, Haifeng Feng, Qian Gao, Xun Xu, Weichang Hao, Xiaolin Wang, C Zhang, Ke-Hui Wu, Shi Xue Dou, Lan Chen, Zhenpeng Hu, and Yi Du

PHYSICS

Realization of flat band with possible nontrivial topology in electronic Kagome lattice

Zhi Li[1]*, Jincheng Zhuang[1,2]*, Li Wang[1], Haifeng Feng[1,2], Qian Gao[3], Xun Xu[1,2], Weichang Hao[2], Xiaolin Wang[1], Chao Zhang[1], Kehui Wu[4,5], Shi Xue Dou[1,2], Lan Chen[4,5†], Zhenpeng Hu[3†], Yi Du[1,2†]

The energy dispersion of fermions or bosons vanishes in momentum space if destructive quantum interference occurs in a frustrated Kagome lattice with only nearest-neighbor hopping. A discrete flat band (FB) without any dispersion is consequently formed, promising the emergence of fractional quantum Hall states at high temperatures. Here, we report the experimental realization of an FB with possible nontrivial topology in an electronic Kagome lattice on twisted multilayer silicene. Because of the unique low-buckled two-dimensional structure of silicene, a robust electronic Kagome lattice has been successfully induced by moiré patterns after twisting the silicene multilayers. The electrons are localized in the Kagome lattice because of quantum destructive interference, and thus, their kinetic energy is quenched, which gives rise to an FB peak in the density of states. A robust and pronounced one-dimensional edge state has been revealed at the Kagome edge, which resides at higher energy than the FB. Our observations of the FB and the exotic edge state in electronic Kagome lattice open up the possibility that fractional Chern insulators could be realized in two-dimensional materials.

INTRODUCTION

In quantum mechanics, the superposition of particle wave functions with unavoidable quantum interference gives birth to new quantum states. Quantum interference associated with frustrated geometry often gives rise to interesting strongly correlated phenomena and the emergence of fascinating nontrivial structures (*1*–*5*). Very recently, a number of works have proven theoretically that completely destructive quantum interference occurs if fermions or bosons are confined in a frustrated Kagome lattice with only nearest-neighbor (NN) hopping (*6*–*13*), as illustrated in Fig. 1A. Consequently, the dispersion relation of the trapped particles exhibits a completely flat characteristic, namely, a flat band (FB), that is, the energy is dispersionless in momentum space. The topologically nontrivial FB can be realized in an electronic Kagome lattice if the non-negligible spin-orbital coupling effect is considered. Consequently, fractional quantum Hall states are expected to emerge when the FB is partially filled (*7*–*9*), because the electronic FB mimics the Landau levels but does not require a magnetic field.

Inspired by these pioneering theoretical predictions, great efforts toward producing artificial Kagome lattices have been undertaken in recent research to examine quantum destructive interference in this frustrated geometry. Although dispersionless plasmons and polaritons have been consecutively realized in corresponding Kagome micro/nanostructures (*14*, *15*), the electronic FB has not been observed, given the challenge in constructing electronic Kagome lattices. For example, molecular Kagome arrangements do not facilitate electronic destructive interference because electron hopping does not follow a Kagome line graph in these structures (*16*, *17*). The ferromagnetic Kagome metal Fe_3Sn_2 is an excellent platform for investigating these exotic electronic properties. Nevertheless, only the massive Dirac fermion characteristics have been identified, and the electronic FB is still unclear in this material (*18*). Recently, a half-filled FB has been achieved in twisted bilayer graphene with a "magic" angle, resulting in correlated insulating states and unconventional superconductivity after the charge carriers are injected (*19*, *20*). This suggests that a new electronic state can be created through manipulating interlayer interactions in two-dimensional (2D) materials by interlayer twisting. Silicene, sharing a similar structure with graphene, exhibits exciting and rich physics and has attracted great interest in recent years (*21*–*23*). Its Dirac electronic structure, chemical stability, and interlayer interactions have been systematically studied (*24*–*28*). As silicon atoms adopt competing sp^2 and sp^3 hybridization states in silicene, they lead to a low-buckled 2D honeycomb structure, which results in a relatively strong interlayer interaction in multilayer silicene. Consequently, the electronic characteristics of multilayer silicene can be significantly modulated by the interlayer interactions, especially in twisted silicene (*28*).

Here, we report the experimental realization of an electronic Kagome lattice with the emergence of an electronic FB on a twisted multilayered silicene surface by using the scanning tunneling microscopy (STM) and scanning tunneling spectroscopy (STS) techniques. The localized electronic states of this FB have been observed and confirmed experimentally. We further reveal that this FB is induced by the electronic Kagome lattice and can induce the edge states even at 77 K, according to STS and density functional theory (DFT). Our work provides an intriguing material candidate for the possible realization of exotic quantum Hall states.

RESULTS

Because of different interactions between silicene and the underlying substrate, abundant silicene phases could be synthesized on Ag(111) (*21*, *22*) that show a strong dependence on the deposition temperature and coverage. After completion of one monolayer, most of the surface area of bilayer and multilayer silicene exhibits a $\sqrt{3} \times \sqrt{3}$ honeycomb reconstruction (in terms of 1×1 silicene) with a lattice constant of 0.64 nm, as shown in Fig. 1 (B and E). The $\sqrt{3} \times \sqrt{3}$ domains are several hundred nanometers in size with a terrace height of 0.31 nm (see fig. S1), which is consistent with previous studies on the 2D multilayer

[1]Institute for Superconducting and Electronic Materials (ISEM), Australian Institute for Innovative Materials (AIIM), UOW-Beihang Joint Research Centre, University of Wollongong, Wollongong, NSW 2525, Australia. [2]Beihang-UOW Joint Research Centre and School of Physics, Beihang University, Beijing 10191, P. R. China. [3]School of Physics, Nankai University, Tianjin 300071, P. R. China. [4]University of Chinese Academy of Sciences, Beijing 100049, P. R. China. [5]Institute of Physics, Chinese Academy of Sciences, Beijing 100190, P. R. China.
*These authors contributed equally to this work.
†Corresponding author. Email: yi_du@uow.edu.au (Y.D.); zphu@nankai.edu.cn (Z.H.); lchen@iphy.ac.cn (L.C.)

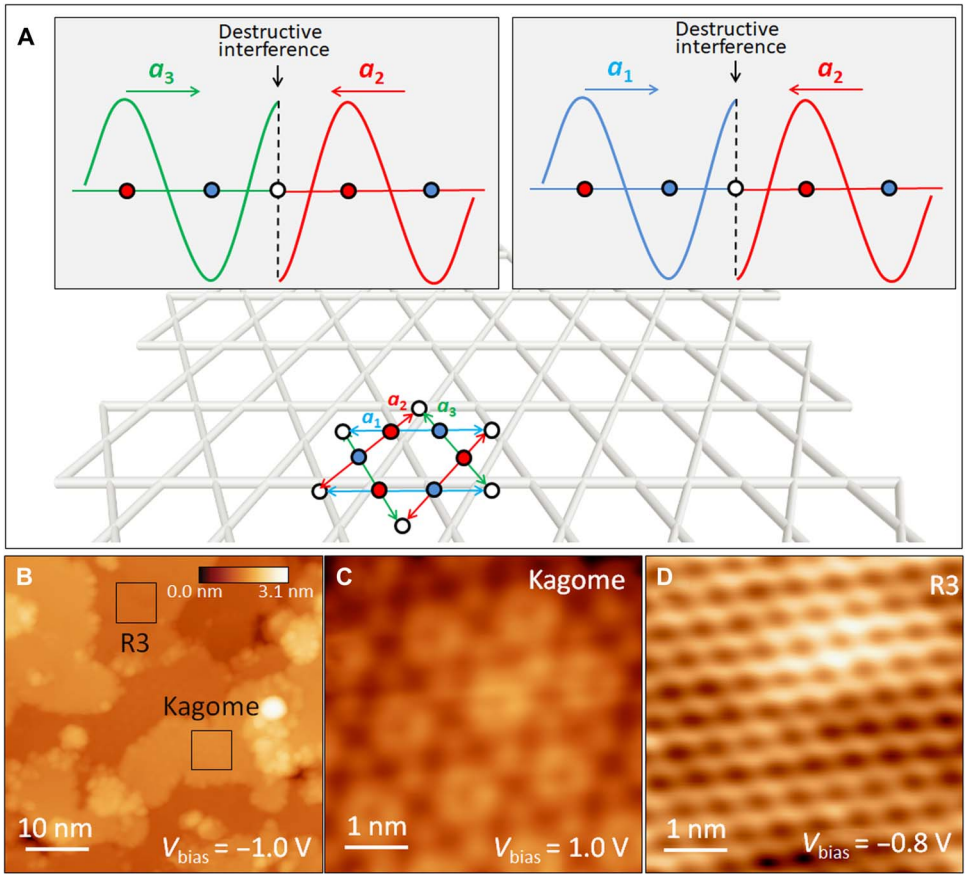

Fig. 1. Kagome lattice imaged by STM. (**A**) Schematic diagram of destructive quantum interference inducing an FB in the Kagome lattice. Three different sites (A, B, and C) are marked with three different colors (blue, white, and red, respectively). The A and C sites have the same wave amplitude, but the A site is antiphase with the C site. Considering only the NN hopping, the possibility of an electron escaping the hexagon is determined by overlapping two hopping vectors, hopping from A to B and from C to B. Because the A and C sites have the same amplitude and the same sign, the two hopping wave vectors will have the same amplitude and opposite signs, as shown in the schematic drawings. Thus, these two vectors will cancel each other out and lead to zero possibility of an electron hopping from the hexagon to the B site, which means that the electrons are localized in the hexagons in the Kagome lattice. In momentum space, the localized electron states mean infinite effective mass and that the energy band is flat. (**B**) STM topographical image (image size, 50 nm × 50 nm; sample bias V_s = 2.7 V; tunneling current I_t = 100 pA) of multilayer silicene (about five layers estimated from the deposition flux) grown on the Ag(111) substrate. (**C**) STM topographical image (5 nm × 5 nm, V_s = 1 V, I_t = 100 pA), giving an enlarged view of the lower right black rectangle in (B) in the Kagome area, with a Kagome lattice constant of 1.7 nm. (**D**) STM topographical image (5 nm × 5 nm, V_s = −0.8 V, I_t = 100 pA), giving an enlarged view of the upper left black rectangle in (B). It shows a honeycomb lattice with a lattice constant of 0.64 nm, which is ascribed to the $\sqrt{3} \times \sqrt{3}$ phase of silicene.

silicene surface (*23*–*27*). A moiré pattern with a lattice constant of 1.7 nm was observed in some $\sqrt{3} \times \sqrt{3}$ domains after interlayer manipulation by the STM tip (*28*). Interlayer twisted $\sqrt{3} \times \sqrt{3}$ bilayer silicene with a twisting angle of 21.8° between the layers induces a $\sqrt{21} \times \sqrt{21}$ superlattice (see fig. S3). In general, the moiré pattern in planar honeycomb materials, for example, graphene, is usually reflected by a hexagonal pattern. In the twisted multilayer silicene, a moiré pattern with the Kagome lattice arrangement was observed, as shown in Fig. 1C. Given the strong interlayer interaction in the twisted $\sqrt{3} \times \sqrt{3}$ silicene multilayer (*28*), the local potential around the AA stacking region should be strongly altered (*29*). The AA stacking of buckling atoms and unbuckled regions are labeled by smaller black plates and larger red plates in Fig. 2F, respectively. The remaining region labeled by blue circles is mainly located between the two nearest black plates. These various local potential regions will act as strong scattering centers, leaving the remaining region as an effective periodical electronic lattice. Therefore, the atom patches labeled by blue circles form a Kagome-like lattice, which is the physical origin of the observed Kagome lattice. At low sample biases ($|V_{bias}| < 0.2$ V), a $\sqrt{3} \times \sqrt{3}$ silicene structure with a faint height modulation can be simultaneously revealed in the Kagome lattice (see fig. S6). This suggests that the observed Kagome lattice in the STM topographic image is not attributable to the silicon atomic lattice but originates from the local density of states (LDOS).

To reveal the detailed LDOS in the Kagome area, we collected *dI*/*dV* tunneling spectra from the sample at different sample positions. Spectra collected in the Kagome area display a broad peak at around 1.7 eV and an intensive single peak at 1.32 eV, which are not detectable from the bare $\sqrt{3} \times \sqrt{3}$ silicene surface, as shown in Fig. 2A. The intensities of both peaks are very much higher than any features in STS on $\sqrt{3} \times \sqrt{3}$ silicene. For instance, their intensities are much higher than the interlayer rotation–induced van Hove singularity (vHs) peaks at −1.2 and 0.75 V (*28*) (as shown in the inset spectra in Fig. 2A), which render the vHs peaks invisible (or negligible) in the *dI*/*dV* tunneling spectra

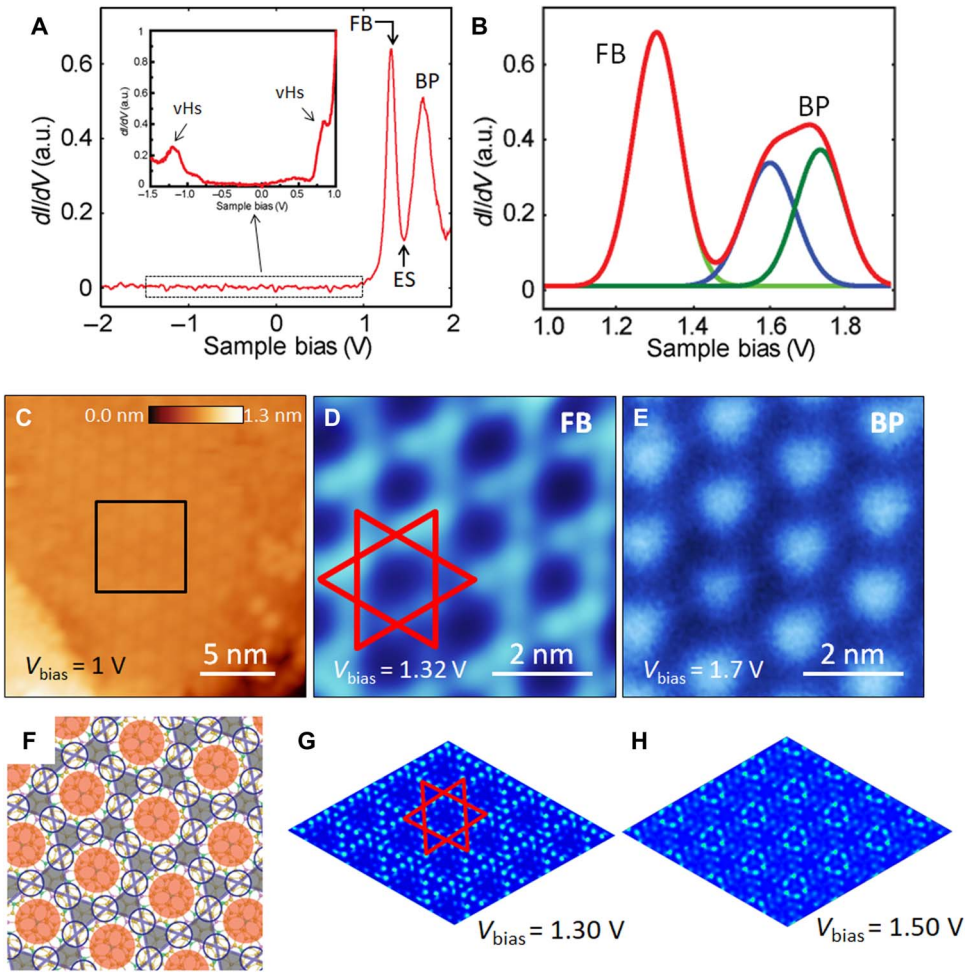

Fig. 2. Electronic structure of the Kagome area. (**A**) STS spectrum (V_s = 2 V, I_t = 100 pA) from the Kagome area shows two distinctive peaks: an intensive peak at 1.32 V (FB peak) and a broad peak (BP) centered around 1.7 V. The valley position corresponds to the energy of Kagome edge state (ES). The inset figure shows the STS spectrum from −1.5 to 1 V (V_s = 1 V, I_t = 100 pA). Two vHs peaks are resolved at −1.2 and 0.75 V. (**B**) Fitting results for the intensive peak and the broad peak. The broad peak is fitted by Lorentzian functions. The two peak components are centered at 1.60 and 1.73 V. (**C**) STM image of large-scale Kagome lattice (20 nm × 20 nm, V_s = 1 V, I_t = 100 pA). (**D** and **E**) DOS mappings of the region enclosed by the black square in (C) at the FB (6 nm × 6 nm, V_s = 1.32 V, I_t = 100 pA) and broad peak (6 nm × 6 nm, V_s = 1.7 V, I_t = 100 pA) energies. (**F**) Structural model of an interlayer twisted silicene multilayer. Two kinds of AA stacking sites are marked by red and black plates, respectively. The red plates are larger than the black plates because of the influence of the larger area of AA stacking sites of unbuckled atoms. The regions not affected have been marked by blue circles. (**G** and **H**) DFT simulation images of LDOS for the FB at around 1.30 V and broad band at around 1.50 V, respectively. The Star of David is a guide to the eye.

in Fig. 2A. This is because the peaks at 1.7 and 1.32 eV are attributable to electronic bands with extremely high DOS. We fitted both peaks by Lorentzian functions to reveal the origins of the corresponding electronic states, as shown in Fig. 2B. For the broad peak at about 1.7 V, two peak components with an interval of 0.13 V were revealed at 1.60 and 1.73 V, respectively. These two components have similar spectral weights, bandwidths, and spectral shapes. The center of the intense single peak is at 1.32 eV. In general, a pronounced single peak with a spectral weight much higher than the vHs peaks in the tunneling spectra indicates band flatness over a large area of the Brillouin zone, which is usually related to two scenarios. The first scenario involves the presence of isolated atoms, defects, or quantum dot systems due to their localized electrons (*30*). At different sample biases, however, from −3 to 3 V, we did not observe any topographical characteristics of isolated atoms, defects, or quantum dots in the STM images of the Kagome area. The first scenario can therefore be ruled out. The second scenario involves localization induced by quantum destructive interference. For instance, the electrons can be localized by destructive interference via multiple hopping paths (*31*), which is the core concept of quantum interference in condensed matter physics. We conducted *dI*/*dV* mapping on the Kagome area at energies of 1.32 and 1.7 V (Fig. 2, D and E), which correspond to the sharp peak and the broad peak, respectively. Coincidently, a clear electronic Kagome pattern is revealed by *dI*/*dV* mapping at the energy exactly corresponding to the peak at 1.32 V, as shown in Fig. 2D. The results suggest that the sharp peak is associated with the frustrated Kagome geometry. The peak with such high intensity is not due to large tunneling matrix elements, because the intensity does not vary with different STM tips or other tunneling parameters in our tunneling spectra (see fig. S8). In contrast, the STS mapping results for the bias range from 1.60 to 1.73 V show a hexagonal pattern (Fig. 2C and fig. S8).

In an electronic Kagome lattice, the behavior of electrons can be understood by the schematic diagram in Fig. 1A. At points A and C, the wave functions are antiphase. If only electronic NN hopping exists, the hopping processes from A to B and from C to B cancel each other out, which effectively localizes the states in the hexagons formed by A and C sites, as shown in Fig. 1A. These localized states manifest themselves as an FB in momentum space. The projection of the FB commonly induces a high-intensity peak in *dI*/*dV* spectra, because it is analogous to high degeneracy of electronic states. On the basis of the above discussion, this suggests that the pronounced peak at 1.32 V is attributable to the electronic localization induced by quantum destructive interference in the Kagome geometry. Furthermore, the observation of a Coulomb pseudo-gap in STS spectra collected from the Kagome area, which is induced by the interaction between the localized electrons and their Coulomb potentials (*32*), confirmed this electronic localization scenario (see fig. S10).

We performed the DFT calculations based on the structural mode of twisted bilayer silicene with a twisting angle of 21.8°, as shown in Fig. 2F. We focused on the spatial distribution of local electron density in the twisted bilayer silicene. Although the electronic band structure is very complex, one can still find two energy windows for the local electron density patterns above 1.0 eV with the same order of energy and a close resemblance to the experimental data. The simulated *dI*/*dV* mappings match the experimental data in terms of the patterns and energy order, which is consistent with both the original Kagome model (Fig. 2, G and H) and the experimental observations (Fig. 2, D and E) and suggests that the expected stacking order is reasonable.

DISCUSSION

To obtain clues to the spatial distributions of the wave functions for the Kagome lattice compared with the experimental *dI*/*dV* mappings, we also performed DFT calculations on an artificial Kagome lattice with three Si atoms (left inset of Fig. 3, $a = b = 6$ Å, $c = 30$ Å, $\alpha = \beta = 90°$, $\gamma = 60°$). As shown in Fig. 3A, the standard Kagome tight-bonding (TB) band features are shown in the three projected bands of the p_z orbitals (marked with red dots), where two Dirac bands (marked with 1 and 2) and one FB (marked with 3) could be identified. The 2D mapping of electron charge densities sampled in the energy range of the Dirac bands and the FB with different energy values are displayed in Fig. 3 (F to H). It is clear that the Kagome-like pattern of local electron charge density exists in either the FB (Fig. 3H) or the Dirac bands (Fig. 3, F and G). Nevertheless, the hexagonal pattern can be observed at an energy level apart from the Kagome bands in this artificial model (marked with 4). The simulated results suggest that the coexistence of the Kagome and hexagonal patterns should be a key

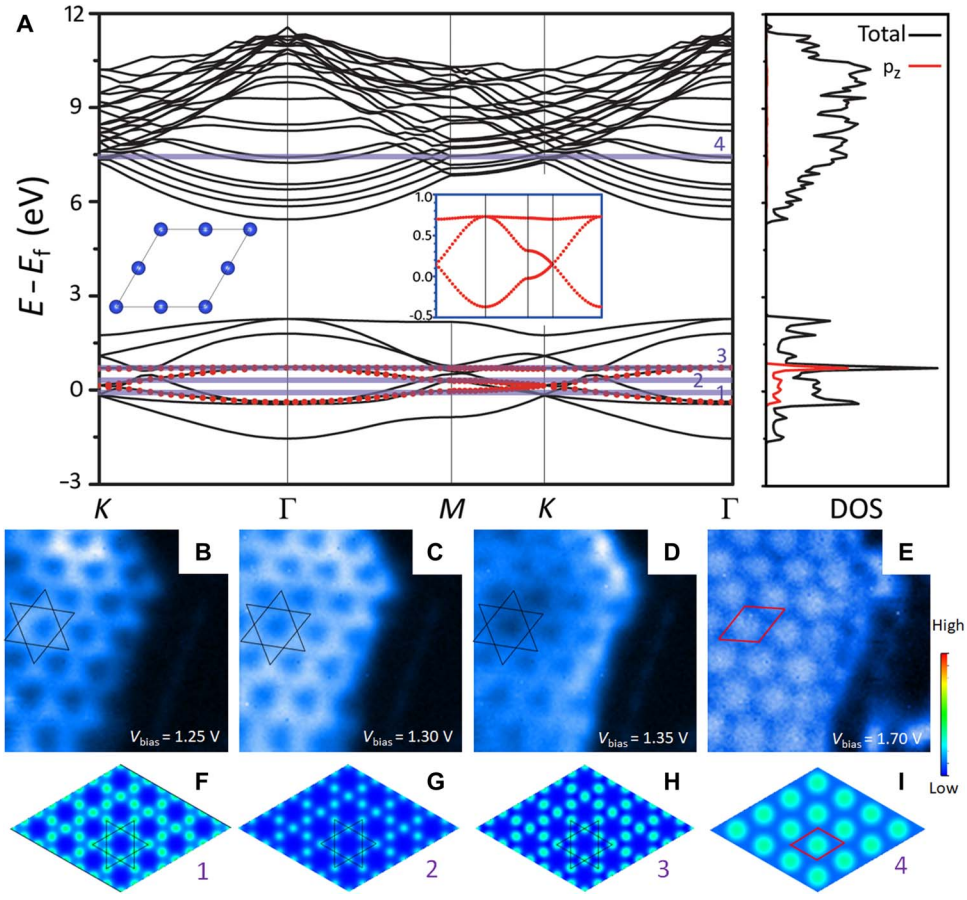

Fig. 3. DFT simulation of electronic Kagome lattice. (**A**) Band structure for a Kagome lattice unit cell made of three Si atoms (left). The right part shows the DOS. Inset of the left panel displays an artificial Kagome lattice with Si atoms (left) and projected p_z bands with one FB and one Dirac cone (right). (**B** to **E**) Experimental *dI*/*dV* maps for the Kagome region with different sample bias: (B) 1.25 V, (C) 1.30 V, (D) 1.35 V, and (E) 1.70 V. (**F** to **I**) Spatial distribution and 2D mapping of the Kagome bands (F to H) and higher band (I) in the band structure (4 × 4 repeated cell). The black Star of David and red rhombus are used as guides to the eye.

feature of the local electronic structure for a Kagome lattice, where the Kagome pattern can be identified in one energy range and the hexagonal pattern is correlated with the energy level higher than the Kagome pattern. The experimental data agree well with these features, as shown in Fig. 3 (B to E). Thus, the FB originates from the formation of the electronic Kagome lattice, and the formation of the BP in Fig. 2B is correlated with the trivial electronic bands, in which its higher intensity is a result of the integration of mixed bands in the deep energy level in Fig. 3A.

The projected DOS (PDOS) is shown in Fig. 3A (right), where the signal from the p_z orbital, which is labeled by the red lines, shows a pronounced peak in the energy level of the FB. In principle, the Dirac band feature could also be observed in the STS data as well as appearing in the PDOS (Fig. 3A). Whether it could be observed or not, however, depends on the energy resolution in the *dI*/*dV* tunneling spectra or the hopping parameter in the TB model. From a Kagome TB model, the band dispersion of the Kagome bands is 3*t*, where *t* is the NN hopping parameter in the electronic Kagome lattice. The value of *t* decreases with an increasing lattice constant of the electronic Kagome lattice, from 1.0 eV (with a lattice constant of 6 Å) to 0.1 eV (with a lattice constant of 9 Å) (see fig. S16). Experimentally, the lattice constant of the electronic Kagome lattice is as large as about 17 Å, where a very small hopping parameter and narrow energy range could be expected. The low intensity and narrow energy range have the result that the features of the Dirac bands become invisible in STS. Therefore, it is reasonable that only a single peak induced by both the Dirac bands and the FB could be identified in *dI*/*dV* tunneling spectra.

Figure 4A shows the topography of the Kagome lattice on a clean $\sqrt{3} \times \sqrt{3}$ silicene surface. As shown in Fig. 4C, the topographical image of the border region reveals a ">" structural terrace edge of the Kagome area, as indicated by the white dotted line. Within the Kagome area, all the complete Kagome lattice cells closest to the terrace edge can be identified. The A, B, and C sites in the complete Kagome lattice cell are labeled by blue, white, and red circles, respectively. When we connected their B sites, a boundary (marked by the black dashed line) that separates incomplete Kagome cells and complete Kagome cells can be seen and is defined as the "Kagome edge" hereafter. In STS mapping in the same region, the spatial distribution of the FB peak at 1.32 V is only confined within the area with complete Kagome lattices (left area to Kagome edge), but it is absent between the Kagome edge and the terrace edge (Fig. 4D and Supplementary Materials). The distance between the Kagome lattice and the terrace edge is about 2 nm in real space, which is significantly larger than the lattice constant of $\sqrt{3} \times \sqrt{3}$ silicene. A ")"-shaped electronic state appears in the STS mapping with a sample bias of 1.45 V, the spatial distribution of which matches perfectly with the Kagome edge (Fig. 4E). This state spreads over several atomic rows with a width of about 2 nm in real space. It is much wider than the edge state induced by edge dangling bonds or atomic reconstructions, which decays exponentially away from the terrace edge (*33*, *34*). There is a clear dangling bond–induced state along the terrace edge with a spatial distribution of less than 1 nm (Fig. 4F). Furthermore, the edge state appears along all island edges with a regular shape in the Kagome lattice region (Fig. 4B and Supplementary Materials). Therefore, the ")"-shaped electronic state at a sample bias of 1.45 V in the STS mapping is

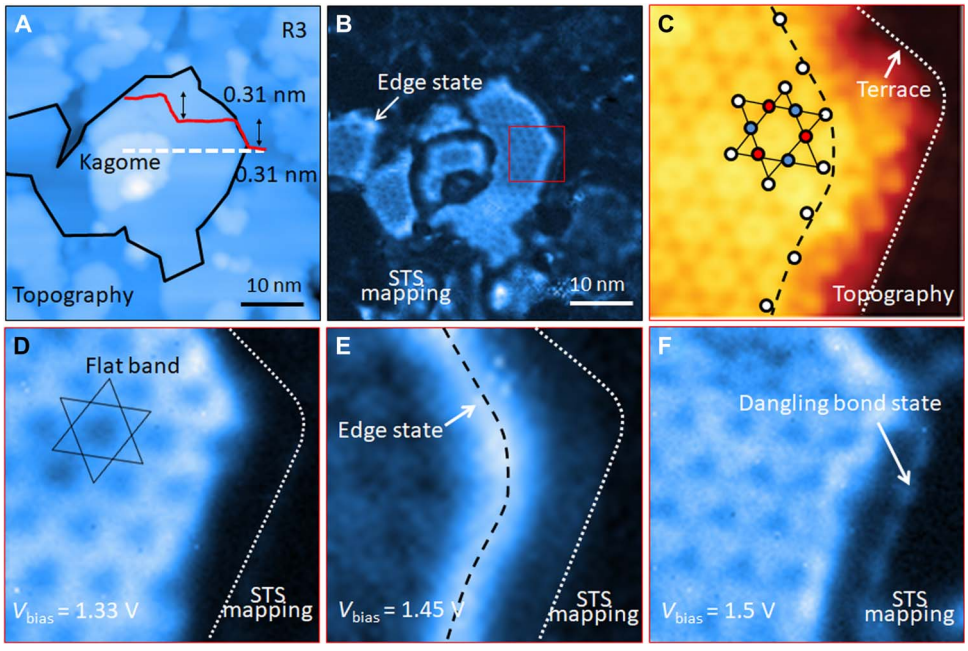

Fig. 4. Electronic structure of Kagome area. (**A**) Large-area image of the Kagome lattice surrounded by $\sqrt{3} \times \sqrt{3}$ silicene (R3 area) (50 nm × 50 nm, V_s = 3 V, I_t = 100 pA). The boundary between them is marked by the black solid line. The red solid line shows the height profile along the white dashed line. The step height is the thickness of one layer of silicene. (**B**) DOS mapping simultaneously obtained at 1.45 V, which is the corresponding edge state energy. The position of the edge state is highlighted by the white arrow. (**C**) Topographical image (10 nm × 10 nm, V_s = 1 V, I_t = 100 pA) of the border region between the Kagome lattice (upper left) and $\sqrt{3} \times \sqrt{3}$ silicene (lower right), which is enclosed by the red square in (B). The Kagome lattice is constructed from three different sites, which are marked by blue, white, and red circles, respectively. The Kagome edge is marked by the black dashed line connecting the white circles. The terrace edge is marked by the white dotted line. (**D** and **E**) DOS mapping of the FB energy (10 nm × 10 nm, V_s = 1.33 V, I_t = 100 pA) reveals the Kagome pattern on the left of these images. The Star of David is a guide to the eye. (E) DOS mapping of the edge state energy (10 nm × 10 nm, V_s = 1.45 V, I_t = 100 pA) shows higher DOS along the dashed line in (C). (**F**) Dangling bonds are revealed by DOS mapping (10 nm × 10 nm, V_s = 1.5 V, I_t = 100 pA).

attributed not to dangling bonds but to the Kagome edge. These mapping results suggest that electronic Kagome geometry gives rise to new electronic edge states due to symmetry breaking in the Kagome lattice.

On the basis of the results and analysis above, the most reasonable picture in physics that we could find may be stated as the following. With the twisting between the Si layers, a screened periodic Coulomb potential field is formed. Then, the nearly free electrons are dominated by the periodic potential, leading to the observation of an electronic Kagome lattice and the FB around 1.3 V, and a hexagonal pattern around 1.7 V. This scenario is also supported by the strong edge state at an energy right above the FB energy (Fig. 2D) at the Kagome edge, which represents the scattering of nearly free electrons on the boundary of the screened periodic Coulomb potential field. This is an inevitable result of broken symmetry in this Kagome system, just as the surface states in semiconductors are always at an energy right above their valence bands. Moreover, it is found that the unique $\sqrt{3} \times \sqrt{3}$ reconstruction could give birth to a ferromagnetic instability, leading to long-range ferromagnetic ordering (*35*). This means that the electronic Kagome lattice observed on multilayer silicene may meet the critical preconditions (Kagome lattice, FB, and magnetism) for exotic topological phenomena, making the observed edge state a promising candidate to realize fractional topological quantum states.

In summary, we experimentally realized an electronic Kagome lattice with the emergence of an electronic FB on a twisted multilayer silicene surface. The local potential modulation attributed to the interlayer interaction gives rise to the generation of an electronic Kagome lattice and, thereby, an electronic FB. The electronic edge state induced by broken symmetry in the Kagome regime has been observed. The present experimental results for the band structure and edge states are consistent with the theoretically predicted topological properties of the Kagome lattice.

MATERIALS AND METHODS

Sample preparation and characterizations

The silicene layers were fabricated by the deposition of silicon atoms on the Ag(111) substrate from a heated silicon wafer in a preparation chamber attached to an in situ STM system under ultrahigh vacuum (UHV; $<1 \times 10^{-10}$ torr). A clean Ag(111) substrate was prepared by argon ion sputtering and subsequently annealed at 820 K for several cycles. The deposition flux of Si was 0.1 monolayer per minute. The temperature of the Ag(111) substrate was kept at 470 K during deposition. The STM and STS measurements were carried out using a low-temperature UHV STM system (STM1500, Unisoku Co.) in UHV at 77 K. The *dI*/*dV* spectroscopy was acquired by switching off the feedback loop and keeping a constant tip-sample distance. The modulation amplitude of 10 mV at 613 Hz was applied, and the corresponding changes in current were measured using a standard lock-in technique.

DFT simulations

All calculations were performed with the Vienna Ab initio Simulation Package (*36*, *37*). The Perdew-Burke-Ernzerhof (PBE) (*38*) functional and a 400-eV cutoff energy on plane-wave basis sets were used in the calculations. A 17.60 Å × 17.60 Å × 30.00 Å unit cell was used for both low-buckled silicene with the H model and the bilayer silicene model to match the $\sqrt{21} \times \sqrt{21}$ geometry. Γ-Centered 5 × 5 × 1 *K*-mesh sampling was used for the cell. Both low-buckled and $\sqrt{3} \times \sqrt{3}$ silicene single-layer models were relaxed until the force on each atom was less than 0.02 eV/Å. Then, the silicon backbone was fixed in the calculations for the H-passivated model and the bilayer model.

SUPPLEMENTARY MATERIALS

Supplementary material for this article is available at http://advances.sciencemag.org/cgi/content/full/4/11/eaau4511/DC1

Fig. S1. Multiple superstructures of silicene on the Ag(111) substrate.
Fig. S2. A 1 × 1 honeycomb structure of $\sqrt{3} \times \sqrt{3}$ silicene.
Fig. S3. Composite moiré pattern for twisted $\sqrt{3} \times \sqrt{3}$ silicene multilayers.
Fig. S4. Kagome lattice formed by composite moiré pattern.
Fig. S5. Comparing twisted multilayer silicene model with STM images.
Fig. S6. High-resolution image of Kagome area shows faint height-modulated $\sqrt{3} \times \sqrt{3}$ silicene structure.
Fig. S7. Kagome lattice on second layer of silicene.
Fig. S8. Ideal STM tunnel junction between tip and twisted $\sqrt{3} \times \sqrt{3}$ silicene multilayer.
Fig. S9. DOS maps in the broad-band bias range.
Fig. S10. Coulomb pseudo-gap.
Fig. S11. Edge state at boundary between Kagome lattice and $\sqrt{3} \times \sqrt{3}$ silicene.
Fig. S12. Edge state located between FB and broad band.
Fig. S13. Absence of FB in imperfect Kagome lattice.
Fig. S14. Spectral distribution in the broken region of the Kagome lattice.
Fig. S15. Electronic structure of Kagome area.
Fig. S16. DFT simulation of artificial Kagome lattice.
Fig. S17. Hexagonal 2D mapping of the local electron density.
Fig. S18. DFT simulation of twisted bilayer silicene.
References (*39*–*42*)

REFERENCES AND NOTES

1. H. Tasaki, Ferromagnetism in the Hubbard models with degenerate single-electron ground states. *Phys. Rev. Lett.* **69**, 1608–1611 (1992).
2. S. Z. Zhang, H.-H. Hung, C. Wu, Proposed realization of itinerant ferromagnetism in optical lattices. *Phys. Rev. A* **82**, 053618 (2010).
3. S. Miyahara, S. Kusuta, N. Furukawa, BCS theory on a flat band lattice. *Phys. C Supercond.* **460–462**, 1145–1146 (2007).
4. C. Wu, D. Bergman, L. Balents, S. Das Sarma, Flat bands and Wigner crystallization in the honeycomb optical lattice. *Phys. Rev. Lett.* **99**, 070401 (2007).
5. C. Wu, S. Das Sarma, $p_{x,y}$-orbital counterpart of graphene: Cold atoms in the honeycomb optical lattice. *Phys. Rev. B* **77**, 235107 (2008).
6. H.-M. Guo, M. Franz, Topological insulator on the kagome lattice. *Phys. Rev. B* **80**, 113102 (2009).
7. E. Tang, J.-W. Mei, X.-G. Wen, High-temperature fractional quantum Hall states. *Phys. Rev. Lett.* **106**, 236802 (2011).
8. K. Sun, Z. Gu, H. Katsura, S. Das Sarma, Nearly flatbands with nontrivial topology. *Phys. Rev. Lett.* **106**, 236803 (2011).
9. T. Neupert, L. Santos, C. Chamon, C. Mudry, Fractional quantum Hall states at zero magnetic field. *Phys. Rev. Lett.* **106**, 236804 (2011).
10. Z. Liu, Z.-F. Wang, J.-W. Mei, Y.-S. Wu, F. Liu, Flat Chern band in a two-dimensional organometallic framework. *Phys. Rev. Lett.* **110**, 106804 (2013).
11. Z. F. Wang, Z. Liu, F. Liu, Organic topological insulators in organometallic lattices. *Nat. Commun.* **4**, 1471 (2013).
12. Z. F. Wang, N. Su, F. Liu, Prediction of a two-dimensional organic topological insulator. *Nano Lett.* **13**, 2842–2845 (2013).
13. Z. Liu, F. Liu, Y.-S. Wu, Exotic electronic states in the world of flat bands: From theory to material. *Chin. Phys. B* **23**, 077308 (2014).
14. Y. Nakata, T. Okada, T. Nakanishi, M. Kitano, Observation of flat band for terahertz spoof plasmons in a metallic kagomé lattice. *Phys. Rev. B* **85**, 205128 (2012).
15. M. Biondi, E. P. van Nieuwenburg, G. Blatter, S. D. Huber, S. Schmidt, Incompressible polaritons in a flat band. *Phys. Rev. Lett.* **115**, 143601 (2015).
16. Q. Chen, S. C. Bae, S. Granick, Directed self-assembly of a colloidal Kagome lattice. *Nature* **469**, 381–384 (2011).
17. K. K. Gomes, W. Mar, W. Ko, F. Guinea, H. C. Manoharan, Designer Dirac fermions and topological phases in molecular graphene. *Nature* **480**, 306–310 (2012).
18. L. Ye, M. Kang, J. Liu, F. von Cube, C. R. Wicker, T. Suzuki, C. Jozwiak, A. Bostwick, E. Rotenberg, D. C. Bell, L. Fu, R. Comin, J. G. Checkelsky, Massive Dirac fermions in a ferromagnetic kagome metal. *Nature* **555**, 638–642 (2018).
19. Y. Cao, V. Fatemi, S. Fang, K. Watanabe, T. Taniguchi, E. Kaxiras, P. Jarillo-Herrero, Unconventional superconductivity in magic-angle graphene superlattices. *Nature* **556**, 43–50 (2018).

20. Y. Cao, V. Fatemi, A. Demir, S. Fang, S. L. Tomarken, J. Y. Luo, J. D. Sanchez-Yamagishi, K. Watanabe, T. Taniguchi, E. Kaxiras, R. C. Ashoori, P. Jarillo-Herrero, Correlated insulator behaviour at half-filling in magic-angle graphene superlattices. *Nature* **556**, 80–84 (2018).
21. P. Vogt, P. De Padova, C. Quaresima, J. Avila, E. Frantzeskakis, M. C. Asensio, A. Resta, B. Ealet, G. Le Lay, Silicene: Compelling experimental evidence for graphenelike two-dimensional silicon. *Phys. Rev. Lett.* **108**, 155501 (2012).
22. B. Feng, Z. Ding, S. Meng, Y. Yao, X. He, P. Cheng, L. Chen, K. Wu, Evidence of silicene in honeycomb structures of silicon on Ag(111). *Nano Lett.* **12**, 3507–3511 (2012).
23. P. De Padova, P. Vogt, A. Resta, J. Avila, I. Razado-Colambo, C. Quaresima, C. Ottaviani, B. Olivieri, T. Bruhn, T. Hirahara, T. Shirai, S. Hasegawa, M. C. Asensio, G. Le Lay, Evidence of Dirac fermions in multilayer silicene. *Appl. Phys. Lett.* **102**, 163106 (2013).
24. P. Vogt, P. Capiod, M. Berthe, A. Resta, P. De Padova, T. Bruhn, G. Le Lay, B. Grandidier, Synthesis and electrical conductivity of multilayer silicene. *Appl. Phys. Lett.* **104**, 021602 (2014).
25. L. Chen, C.-C. Liu, B. Feng, X. He, P. Cheng, Z. Ding, S. Meng, Y. Yao, K. Wu, Evidence for Dirac fermions in a honeycomb lattice based on silicon. *Phys. Rev. Lett.* **109**, 056804 (2012).
26. E. Salomon, R. E. Ajjouri, G. Le Lay, T. Angot, Growth and structural properties of silicene at multilayer coverage. *J. Phys. Condens. Matter* **25**, 185003 (2014).
27. P. De Padova, C. Ottaviani, C. Quaresima, B. Olivieri, P. Imperatori, E. Salomon, T. Angot, L. Quagliano, C. Romano, A. Vona, M. Muniz-Miranda, A. Generosi, B. Paci, G. Le Lay, 24h stability of thick multilayer silicene in air. *2D Mater.* **1**, 021003 (2014).
28. Z. Li, J. Zhuang, L. Chen, Z. Ni, C. Liu, L. Wang, X. Xu, J. Wang, X. Pi, X. Wang, Y. Du, K. Wu, S. X. Dou, Observation of van Hove singularities in twisted silicene multilayers. *ACS Cent. Sci.* **2**, 517–521 (2016).
29. K. Uchida, S. Furuya, J.-I. Iwata, A. Oshiyama, Atomic corrugation and electron localization due to Moiré patterns in twisted bilayer graphenes. *Phys. Rev. B* **90**, 155451 (2014).
30. L. Feng, X. Lin, L. Meng, J.-C. Nie, J. Ni, L. He, Flat bands near Fermi level of topological line defects on graphite. *Appl. Phys. Lett.* **101**, 113113 (2012).
31. P. W. Anderson, Absence of diffusion in certain random lattices. *Phys. Rev.* **109**, 1492–1505 (1958).
32. M. Morgenstern, D. Haude, J. Klijn, R. Wiesendanger, Coulomb pseudogap caused by partial localization of a three-dimensional electron system in the extreme quantum limit. *Phys. Rev. B* **66**, 121102 (2002).
33. C. Tao, L. Jiao, O. V. Yazyev, Y.-C. Chen, J. Feng, X. Zhang, R. B. Capaz, J. M. Tour, A. Zettl, S. G. Louie, H. Dai, M. F. Crommie, Spatially resolving edge states of chiral graphene nanoribbons. *Nat. Phys.* **7**, 616–620 (2011).
34. K. Ambal, P. Rahe, A. Payne, J. Slinkman, C. C. Williams, C. Boehme, Electrical current through individual pairs of phosphorus donor atoms and silicon dangling bonds. *Sci. Rep.* **6**, 18531 (2016).
35. H. Fu, Z. Liu, C. Lian, J. Zhang, H. Li, J.-T. Sun, S. Meng, Magnetic Dirac fermions and Chern insulator supported on pristine silicon surface. *Phys. Rev. B* **94**, 035427 (2016).
36. G. Kresse, J. Furthmüller, Efficiency of ab-initio total energy calculations for metals and semiconductors using a plane-wave basis set. *Comput. Mater. Sci.* **6**, 15–50 (1996).
37. G. Kresse, J. Furthmüller, Efficient iterative schemes for ab initio total-energy calculations using a plane-wave basis set. *Phys. Rev. B* **54**, 11169–11186 (1996).
38. J. P. Perdew, K. Burke, M. Ernzerhof, Generalized gradient approximation made simple. *Phys. Rev. Lett.* **77**, 3865–3868 (1996).
39. Y. Du, J. Zhuang, H. Liu, X. Xu, S. Eilers, K. Wu, P. Cheng, J. Zhao, X. Pi, K. W. See, G. Peleckis, X. Wang, S. X. Dou, Tuning the band gap in silicene by oxidation. *ACS Nano* **8**, 10019–10025 (2014).
40. J. Chen, Y. Du, Z. Li, W. Li, B. Feng, J. Qiu, P. Cheng, S. X. Dou, L. Chen, K. Wu, Delocalized surface state in epitaxial Si(111) film with spontaneous $\sqrt{3} \times \sqrt{3}$ superstructure. *Sci. Rep.* **5**, 13590 (2015).
41. J. Zhuang, X. Xu, H. Feng, Z. Li, X. Wang, Y. Du, Honeycomb silicon: A review of silicene. *Sci. Bull.* **60**, 1551–1562 (2015).
42. L. Gross, N. Moll, F. Mohn, A. Curioni, G. Meyer, F. Hanke, M. Persson, High-resolution molecular orbital imaging using a *p*-wave STM tip. *Phys. Rev. Lett.* **107**, 086101 (2011).

Acknowledgments: We thank T. Silver for valuable comments on this work. We also thank X.-G. Wen (Massachusetts Institute of Technology), F. Liu (University of Utah), and Z. Liu (Tsinghua University) for valuable discussions on this work. **Funding:** This work was supported by the Australian Research Council (ARC) through Discovery Projects (DP140102581, DP160102627, DP170101467, and FT180100585) and Linkage Infrastructure, Equipment and Facilities (LIEF) grants (LE100100081 and LE110100099). Z.L. would like to acknowledge support from the University of Wollongong through the Vice Chancellor's Postdoctoral Research Fellowship Scheme. Z.H. would like to acknowledge the China Scholarship Council (CSC) for financial support (no. 201506200150). The work was partially supported by the National Natural Science Foundation of China (grant nos. 11334011, 11322431, 11304368, 11674366, 11674368, 21773124, 11874003, and 21203099), the Fok Ying Tung Education Foundation (no. 151008), and the Strategic Priority Research Program of the Chinese Academy of Sciences (grant no. XDB07020100). The calculations were performed on the Tianhe-2 supercomputer in the National Supercomputing Center in Guangzhou. The staff from the supercomputing center and the engineers from Beijing Paratera Technology Co. Ltd. provided efficient support to make the work proceed smoothly. **Author contributions:** Z.L., J.Z., and Y.D. designed the experimental plan. Z.L. and L.C. prepared the samples. Z.L., J.Z., H.F., and Y.D. did STM characterizations. Z.H. carried out modeling and DFT calculations. L.W., X.X, X.W., C.Z., K.W., W.H., and S.X.D. helped with data analysis. All authors participated in discussions on the data. Z.L., Z.H., and Y.D. wrote the paper. **Competing interests:** The authors declare that they have no competing interests. **Data and materials availability:** All data needed to evaluate the conclusions in the paper are present in the paper and/or the Supplementary Materials. Additional data related to this paper may be requested from the authors.

Submitted 12 June 2018
Accepted 16 October 2018
Published 16 November 2018
10.1126/sciadv.aau4511

Citation: Z. Li, J. Zhuang, L. Wang, H. Feng, Q. Gao, X. Xu, W. Hao, X. Wang, C. Zhang, K. Wu, S. X. Dou, L. Chen, Z. Hu, Y. Du, Realization of flat band with possible nontrivial topology in electronic Kagome lattice. *Sci. Adv.* **4**, eaau4511 (2018).

Realization of flat band with possible nontrivial topology in electronic Kagome lattice

Zhi Li, Jincheng Zhuang, Li Wang, Haifeng Feng, Qian Gao, Xun Xu, Weichang Hao, Xiaolin Wang, Chao Zhang, Kehui Wu, Shi Xue Dou, Lan Chen, Zhenpeng Hu and Yi Du

Sci Adv **4** (11), eaau4511.
DOI: 10.1126/sciadv.aau4511